Article

Improving BeiDou Global Navigation Satellite System (BDS-3)-Derived Station Coordinates Using Calibrated Satellite Antennas and Station Inter-System Translation Parameters

Tao Zhang [1,2], Shiwei Guo [2,3,*], Lei Fan [2,3] and Chuang Shi [2,3]

[1] School of Electronic and Information Engineering, Beihang University, Beijing 100083, China; buaa_zt@buaa.edu.cn
[2] Key Laboratory of Navigation and Communication Fusion Technology, Ministry of Industry and Information Technology, Beijing 100083, China; bhflei@buaa.edu.cn (L.F.); shichuang@buaa.edu.cn (C.S.)
[3] School of Space and Earth Science, Beihang University, Beijing 100083, China
* Correspondence: guosw@buaa.edu.cn

Abstract: The BeiDou global navigation satellite system (BDS-3) has been widely applied in various geodetic applications since its full operation. However, the estimated station coordinates using BDS-3 are less precise compared to GPS results. It contains systematic errors caused by scale bias with respect to International GNSS Service (IGS) 2020 frame and Inter-System Translation Parameters (ISTPs). In order to improve the consistency of BDS-3-derived station coordinates with respect to IGS20 products, we firstly estimated the satellite antenna Phase Center Offsets (PCOs) for BDS-3 Medium Earth Orbit (MEO) constellation, and then estimated station-specific ISTPs from GPS to BDS-3 systems. The results indicate that the PCO-Z estimates show large differences among satellites from different manufacturers and orbit planes. The estimated BDS-3 satellite PCOs exhibit a systematic bias of −9.3 cm in the Z-direction compared to ground calibrations. The maximum mean station-specific ISTPs can reach up to 3 mm, highlighting significant variability and the need for refinement in positioning. When using the estimated PCOs instead of igs20.atx values, the estimated scale bias with respect to the IGS20 frame is reduced from 0.38 ppb to −0.12 ppb, indicating that the refined BDS-3 satellite PCOs are well compatible with IGS20. Regarding the Up component that is correlated with the scale factor, the station coordinate differences with respect to the IGS20 frame is reduced from 7.0 mm to 6.2 mm in terms of the root mean square (RMS), which is improved by 11.4%. Considering the additional ISTP corrections, a further improvement of 17% was obtained in station coordinates. The RMS of station coordinate differences with respect to the IGS20 frame is 2.3 mm, 2.7 mm, and 5.2 mm for the North, East, and Up components, respectively.

Keywords: BDS-3; PCO; inter-system translation parameters; terrestrial scale; IGS20

1. Introduction

The BDS-3 [1], since it became fully operational, has been widely applied in various earth science research areas, including the achievement of terrestrial reference frame scale [2] and the determination of geocenter motion and Earth Rotation Parameters (ERPs) [3,4]. An essential requirement for these geodetic applications is the precise estimation of station coordinates [5,6], which serves as a critical foundation for the scientific analysis of geophysical signals and processes. Nowadays, the static positioning accuracy of BDS-3

with the Precise Point Positioning (PPP) method [7] stays at the level of 3 mm and 7 mm for the horizontal and vertical components, respectively, which is worse than the established GPS results of 2–3 mm and 4 mm [8]. This comparison suggests that the estimated station coordinates by using BDS-3 suffer from some potential modeling issues.

Currently, the International GNSS Service (IGS) [9] operational products have incorporated the IGS20/igs20.atx framework [10], where the Z component of Phase Center Offset (PCO-Z) of all GPS, GLONASS, and Galileo satellite antennas are aligned to the ITRF2020 [10], while the PCO-Z of BDS-3 constellation is based on the ground calibrations published by the China Satellite Navigation Office (CSNO) [11]. This strategy entails two primary risks. First, the PCO values provided by the CSNO may deviate from actual values due to environmental factors and manufacturing variations [12]. Second, these a priori values may not be fully compatible with the ITRF scale [13]. Zhu et al. [14] demonstrated the strong correlation between satellite PCO-Z, terrestrial scale, and station height. Moreover, ref. [13] showed that the inconsistency of scales between BDS and Galileo was at the level of about +1.854 ± 0.191 ppb. Therefore, it is crucial to determine PCOs for BDS-3 satellites that are consistent with the IGS20 scale, as discrepancies in scale directly affect the accuracy of station coordinates. Bridging this gap ensures a unified scale across different solutions, enhancing the precision and consistency of positioning. Although several studies have made efforts to estimate BDS-3 satellite PCOs [2,12,13,15,16], their results are based on the outdated igs14.atx or igsR3.atx, which were not consistent with the IGS20 scale. Huang [16] estimated the BDS-3 satellite PCOs within the IGS14 reference frame using long-term data and receiver antenna calibrations, highlighting the sensitivity of PCO estimates to calibration models and their impact on positioning accuracy. Recently, only Yuan [17] presented the PCO estimates for BDS-3 satellites aligned to the IGS20 frame. In their study, the station coordinates used for scale definition were simply fixed to the IGS20 coordinates. This type of strong constraint, although highly effective in addressing the rank deficiency problem of the normal equations, may cause deformation in the geodetic control network due to its rigid enforcement. An alternative method to define the terrestrial scale information is by using the minimal constraints, namely, the No-Net-Scale (NNS) constraints, which only introduce an external reference for terrestrial scale and do not affect the internal structure of the network. Nevertheless, comprehensive research verifying the influence of the aligned BDS-3 satellite PCOs on the accuracy of station coordinates remains insufficient and requires further investigation. Additionally, it would be beneficial to have an independent PCO results for comparison and validation of BDS-3 based terrestrial scale.

In addition to satellite PCOs, the so-called Inter-System Translation Parameters (ISTPs) [18] also affect the consistency of station coordinates determined by different GNSS constellations. The ISTPs are defined as the discrepancy between two GNSS coordinates, which may result from discrepancies in receiver antenna calibrations and also may be influenced by other factors such as the troposphere [19]. Notably, some studies [19,20] established similar bias parameters that generally include two parts, receiver antenna vector and troposphere bias. Following Villiger [18], the station-specific ISTPs in this study only refer to the translation vector of receiver antenna calibrations, which are expressed in the local horizon system at each station. Within the life of IGS14/igs14.atx framework [21], the GPS-specific receiver antenna calibrations have been applied to BDS-3/Galileo due to lack of available BDS/Galileo-specific receiver antenna calibrations, creating a potential source of inconsistency for station coordinates. Moreover, when using the Galileo satellite antenna calibrations published by GSA together with the GNSS-specific receiver antenna calibrations from igsR3.atx, Dach [22] observed significant inter-GNSS translation biases of 7.5 mm for Galileo relative to GPS, and Villiger [23] found a similar bias in the scale with respect to the IGS14 frame. There happens to be a similar

case for BDS-3 in the new IGS20/igs20.atx framework. Though BDS-specific receiver antenna calibrations are available, BDS-3 satellite antenna corrections are still from CSNO, which is not compatible with other GNSS values adjusted to the terrestrial scale of ITR2020. Therefore, taking the ISTP into consideration is of great significance in order to evaluate the BDS-specific receiver antenna calibrations and improve the consistency of BDS-based terrestrial scale with respect to the IGS20 frame.

Typically, it is widely accepted that the station coordinates derived by GPS are more reliable than those by BDS-3 or any other navigation systems. Taking GPS results as a reference, this study aims to improve the BDS-3-derived station coordinates and the resulting scale consistency with respect to the IGS20 frame in terms of the following two aspects. Firstly, satellite antenna PCOs for BDS-3 MEO constellation are estimated in the IGS20/igs20.atx framework by constraining the terrestrial scale through a NNS condition with respect to the daily station coordinates in the IGS20 frame. Secondly, the station-specific ISTPs from GPS to BDS-3 systems are estimated and then modeled for each station with the adjusted BDS-3 MEO satellite antenna PCOs. The paper is organized as follows. Section 2 outlines the methodology for estimating PCOs and ISTPs, and details the processing strategy. Section 3 presents the analysis of the estimated PCO and ISTP results, providing a review of the findings and their implications. Additionally, PPP solutions were conducted to evaluate the impact of the estimated PCO and ISTP results. The summary and conclusion are given in the last section.

2. Methods

This section introduces the methodology for estimating the satellite antenna PCOs and the station-specific ISTPs. Additionally, the detailed data processing strategies are summarized.

2.1. Estimation of Satellite Antenna PCO

The satellite PCO, defined in the spacecraft body fixed system (SBF), comprises three components: PCO-X, PCO-Y, and PCO-Z [24]. These offsets are linked to the mechanical structure of the satellite, with the origin coinciding with the satellite's center of mass (COM). The PCO-Z axis points toward the geocenter, while the PCO-Y axis, aligned with the solar panels' rotation axis, is defined as the cross product of the PCO-Z axis and the vector from the satellite to the Sun. The PCO-X axis completes the right-handed coordinate system [25].

The PCO vector in the inertial coordinate system (ICS) $\mathbf{P}_{ics}$ can be expressed as follows:

$$\mathbf{P}_{ics} = \mathbf{R}_{sbf \to ics} \cdot \mathbf{P}_{sbf} = \begin{pmatrix} e_X & 0 & 0 \\ 0 & e_Y & 0 \\ 0 & 0 & e_Z \end{pmatrix} \begin{pmatrix} \Delta x \\ \Delta y \\ \Delta z \end{pmatrix} \tag{1}$$

where $\mathbf{P}_{sbf} = (\Delta x, \Delta y, \Delta z)^T$ is the PCO vector in the SBF, and $\mathbf{R}_{sbf \to ics} = diag(e_X \quad e_Y \quad e_Z)$ is the rotation matrix that transforms coordinates from the SBF to the inertial coordinate system. $diag(e_X \quad e_Y \quad e_Z)$ are the components of the rotation matrix vector of the coordinate axes under the SBF.

Taking the influence of the satellite PCOs into account, the geometric distance from the satellite to the station can be written as follows:

$$R_k^s = \left\| \mathbf{r}^{s,ant} - \mathbf{r}_k^{ant} \right\| = \left\| \mathbf{r}^{s,com} + \mathbf{R}_{sbf \to ics} \cdot \mathbf{P}_{sbf} - \mathbf{r}_k^{ant} \right\| \tag{2}$$

where R_k^s is the range of station k to the antenna phase center of satellite s. $\|\cdot\|$ represents the norm of the vector. $\mathbf{r}^{s,ant}$ is the position of the satellite antenna phase center. $\mathbf{r}^{s,com}$ and $\mathbf{r}_k^{ant}$ are the positions of the satellite center of mass and the receiver antenna phase center.

The partial derivative equation for the satellite PCO parameters can be expressed as follows:

$$\frac{\partial R_k^s}{\partial P_{sbf}} = \frac{\mathbf{r}^{s,com} + \mathbf{R}_{sbf \to ics} \cdot \mathbf{P}_{sbf} - \mathbf{r}_k^{ant}}{\left(\mathbf{r}^{s,com} + \mathbf{R}_{sbf \to ics} \cdot \mathbf{P}_{sbf} - \mathbf{r}_k^{ant}\right)^T \cdot \left(\mathbf{r}^{s,com} + \mathbf{R}_{sbf \to ics} \cdot \mathbf{P}_{sbf} - \mathbf{r}_k^{ant}\right)} \cdot \mathbf{R}_{sbf \to ics} \quad (3)$$

2.2. Estimation of Station-Specific ISTPs

The ISTPs with respect to receiver antenna calibrations are expressed in the local horizon system at each station. The North direction is aligned with the semi-minor axis of the Earth's ellipsoid. The East direction is aligned with the semi-major axis of the Earth's ellipsoid. The Up direction is aligned with the Earth's ellipsoidal normal. In practice, the distance correction from satellite to station caused by the station-specific ISTPs can be formulated as follows:

$$ISTP_{ecef} = R_{neu \to ecef} \cdot \begin{pmatrix} \Delta n_k \\ \Delta e_k \\ \Delta u_k \end{pmatrix} \quad (4)$$

$$ISTP_{ics} = R_{ecef \to ics} \cdot ISTP_{ecef} \quad (5)$$

where $ISTP = \begin{pmatrix} \Delta n_k & \Delta e_k & \Delta u_k \end{pmatrix}^T$ is the station ISPT vector in the local horizon system, $ISTP_{ics}$ is the station ISTP in the inertial coordinate system, $R_{neu \to ecef}$ is the rotation matrix from the local horizon system to the Earth-Centered Earth-Fixed (ECEF) system, and the $R_{ecef \to ics}$ represents the rotation matrix from the ECEF to the inertial coordinate system.

$$R_k^s = \left\| \mathbf{r}^{s,ant} - \mathbf{r}_k^{ant} \right\| = \left\| \mathbf{r}^{s,com} - \mathbf{r}_k^{ant} - ISTP_{ics} \right\| \quad (6)$$

The partial derivative of the observation with respect to ISTP parameters can be expressed as follows:

$$\frac{\partial R_k^s}{\partial ISTP} = \frac{\mathbf{r}^{s,com} - \mathbf{r}_k^{ant} - R_{ecef \to ics} \cdot R_{enu \to ecef} \cdot ISTP}{\left(\mathbf{r}^{s,com} - \mathbf{r}_k^{ant} - R_{ecef \to ics} \cdot R_{enu \to ecef} \cdot ISTP\right)^T \cdot \left(\mathbf{r}^{s,com} - \mathbf{r}_k^{ant} - R_{ecef \to ics} \cdot R_{enu \to ecef} \cdot ISTP\right)} \cdot R_{ecef \to ics} \cdot R_{enu \to ecef} \quad (7)$$

2.3. Data Collection and Processing Strategy

The general data processing tasks in this study include two key parts, namely, the estimation of satellite antenna PCOs and station-specific ISTPs. Figure 1 presents the steps of the data processing workflow. All data processing was performed within the IGS20/igs20.atx framework by using the Geodetic Spatial Temporal data Analysis and Research (GSTAR) version 1.0 software [26] developed at Beihang University. Considering that the IGS20 reference frame is a global framework, ensuring better consistency is a priority. The primary roles of BDS-3 Geostationary (GEO) and Geosynchronous Orbit (IGSO) satellites are to increase the number of visible observations in the Asia-Pacific region and broadcast corrections, thereby improving regional service performance. Due to the relatively poor orbit accuracy and regional coverage constraints of the BDS-3 IGSO and GEO

satellites [27], our analysis focuses exclusively on BDS-3 MEO satellites to ensure the highest quality of results.
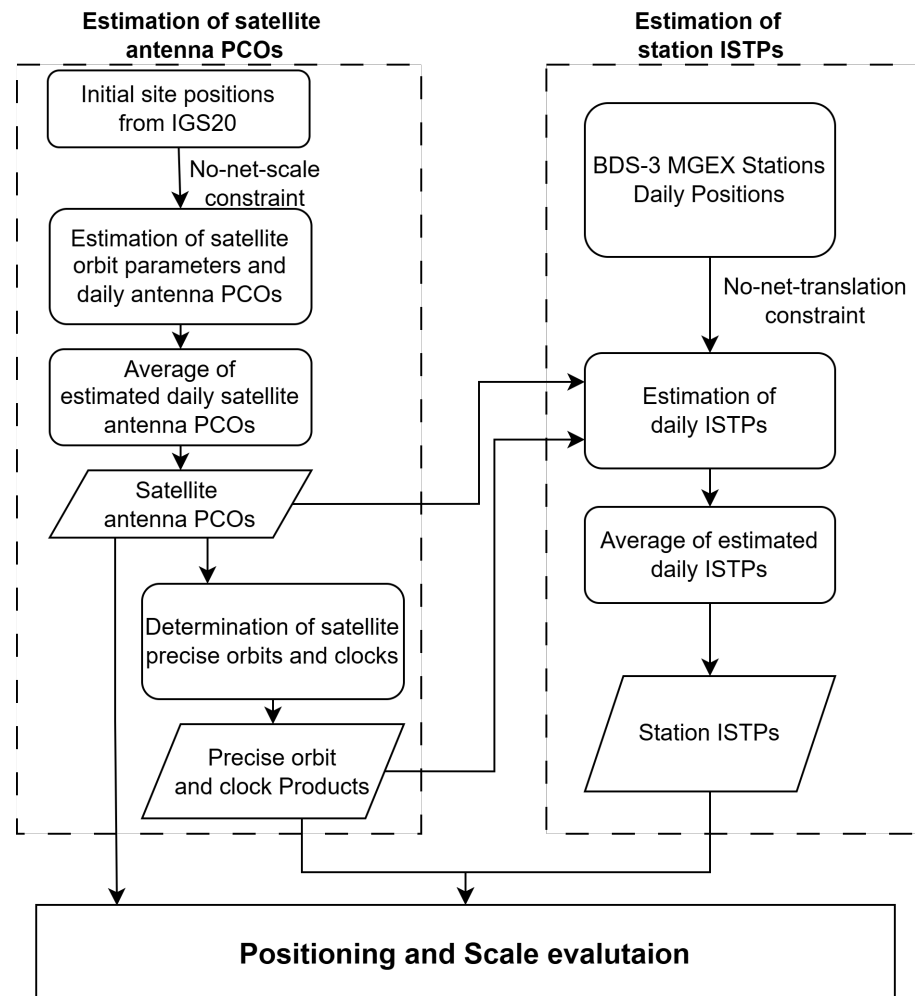
Figure 1. The data processing workflow for the determination of satellite antenna PCOs and station-specific ISTPs.

　　The satellite antenna PCOs of BDS-3 MEO constellation were firstly estimated from precise orbit determination (POD) solutions in daily batches. A total of 99 global stations tracking all BDS-3 MEO and GPS satellites were selected from IGS Multi-GNSS Experiment (MGEX) network [28]. Figure 2 shows the distribution of the selected stations for PCOs' estimation, which are marked in red. The undifferenced ionosphere-free (IF) code and carrier phase observations of B1I and B3I signals were processed with the 300 s sampling throughout the year of 2023. The IGS20 scale was introduced by applying an NNS condition to the core station coordinates from IGS daily combined solutions [29]. The daily estimated PCOs were then averaged to obtain a constant value for each satellite, with any values exceeding the three-sigma threshold excluded from the averaging process. With the resulting BDS-3 satellite antenna PCOs and GPS satellite antenna models from IGS20.atx, a joint POD solution combining BDS-3 and GPS satellites was reprocessed throughout 2023 by using the aforementioned 99 global stations to derive precise satellite orbits and clocks. Concerning the POD in this study, the seven-parameter extended Empirical CODE Orbit Model (ECOM2) [30] was used for BDS-3 and GPS satellite orbit dynamic modeling. The detailed data processing strategies are listed in Table 1.
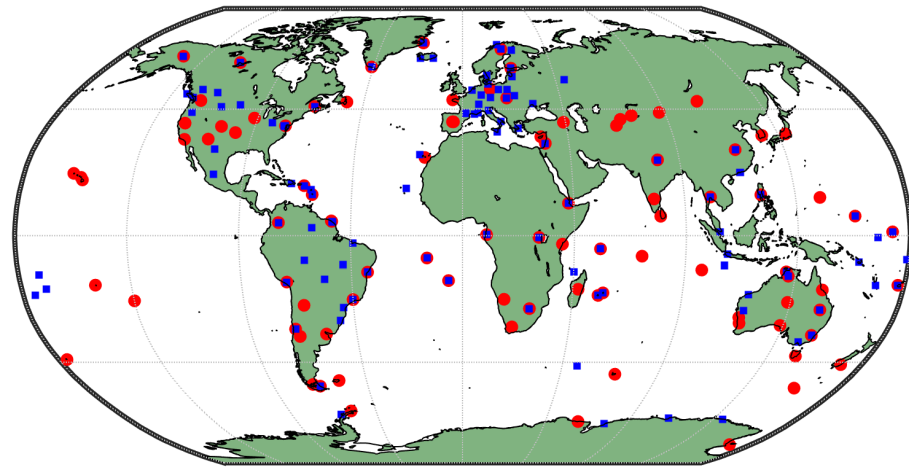
Figure 2. The global distribution of BDS-3 tracking stations. The red point is for the estimation of satellite antenna PCOs, and the blue point is for the estimation of station-specific ISTPs.

Table 1. Strategies for PCOs' and ISTPs' estimation.

Items	Strategy
Constellation	BDS-3 MEO satellites GPS
Observation	Undifferenced ionosphere-free linear combination of code and phase measurements on BDS-3 B1I/B3I and GPS L1 C/A/L2 P(Y)
Time span	1 January 2023~31 December 2023
Sample rate	300 s
Session length	24 h
Cutoff elevation	7°
Earth gravity	Earth Gravitational Model 2008 (EGM2008) (12 × 12) (Pavlis et al., 2008 [31])
N-body gravity	Sun, moon, and planets with coordinates from Jet Propulsion Laboratory (JPL) Development Ephemerides (DE405) ephemeris (Standish, 1998 [32])
Ocean tide	Finite Element Solution 2004 (FEL2004) tide model (Lyard et al., 2006 [33])
Tide forces and relativistic effects	Models refer to IERS conventions 2010 (Petit & Luzum, 2010 [34])
Earth radiation pressure	Models refer to Rodriguez-Solano et al. (2012b) [35]
Antenna thrust	Models refer to [36]
Solar radiation pressure (SRP)	Seven-parameter ECOM2 for BDS and GPS satellites
Satellite antenna calibrations	BDS-3: initial values are from igs20_2247.atx while corrections are estimated as constants. GPS: igs20_2247.atx
Receiver antenna calibrations	igs20_2247.atx
Station coordinate	Tightly constrained to IGS daily solutions
Troposphere delay	Priori value using GPT2 and Saastamoinen model (Saastamoinen, 1972 [37]) with VMF1 mapping function (Boehm et al., 2006 [38]; Lagler et al., 2013 [39]); residual wet ZPD is estimated as 1 h constant and horizontal gradients are estimated as 24 h constants.
Ambiguity	Double-differenced ambiguity resolution [40]

With these reprocessed satellite antenna PCOs for BDS-3 MEO constellation and precise products for BDS-3 and GPS satellites, the station-specific ISTPs from the GPS to the BDS-3 phase center of the same station were estimated from daily PPP solutions. The undifferenced IF observations collected from 118 stations tracking both BDS-3 MEO and GPS satellites were processed in this procedure during the same period as that employed for satellite antenna PCOs' estimation. The distribution of these stations is shown in Figure 2 and is marked in blue. The selected 118 stations cover a total of 16 different types of receiver antennas, which are well calibrated for research analysis, as listed in Table 2. Station coordinates were constrained by the no-net-translation (NNT) condition to the IGS20 daily coordinates. The final ISTPs for each station were derived by averaging daily station-specific ISTP estimates, where any estimate with a value larger the three-sigma threshold was considered to be an outlier and was excluded. Apart from the processing strategies dedicated for POD solutions, the same background models were employed in PPP solutions, which are presented in Table 1.

Table 2. Ground station receiver antenna types used in ISTP estimation.

Antenna	Radome	Antenna	Radome
ASH700936D_M	SCIS	SEPCHOKE_B3E6	SPKE
ASH701945B_M	SCIS	TPSCR.G3	SCIS
ASH701945C_M	NONE	TPSCR.G5	TPSH
ASH701945E_M	SCIS	TRM115000.00	NONE
JAVRINGANT_DM	NONE	TRM55971.00	NONE
LEIAR20	LEIM	TRM57971.00	NONE
LEIAR20	NONE	TRM59800.00	NONE
LEIAR25.R3	LEIT	TRM59800.00	SCIS
LEIAR25.R4	LEIT	TRM59800.00	SCIT
LEIAR25.R4	NONE	TRM59800.80	SCIT

3. Results and Discussion

This section focuses on the analysis of the estimated satellite antenna PCOs of BDS-3 MEO constellation and on the modeling of station-specific ISTPs from GPS to BDS-3 systems. For evaluation purpose, stations coordinates were derived from PPP solutions by using the estimated PCOs and ISTPs, and then were evaluated by comparing them to IGS daily results. Moreover, the terrestrial scales derived from different processing schemes were analyzed to assess the consistency of the estimated BDS-3 satellite PCOs with the IGS20 frame.

3.1. Estimation of BDS-3 MEO Satellite PCOs

In principle, the formal errors of PCO parameters in the covariance matrix obtained through Least Squares (LSQ) estimation represent the estimated uncertainty, mainly reflecting the determinability of PCO parameters due to the Sun–Earth–satellite geometry [2]. This process is based on the theoretical framework outlined in Section 2.1, where the observation models and parameter estimation are defined. Figure 3 illustrates the formal errors of BDS-3 satellite PCO estimates as a function of the Sun elevation angles above orbital planes (β). These formal errors reflect the precision of the estimated PCOs. Two typical satellites, one is C19 from the China Academy of Space Technology (CAST) manufacturer (left panel) and the other is C29 from the Shanghai Engineering Center for Microsatellites (SECM) manufacturer (right panel), are selected. For the C19 satellite, the formal errors of PCO-X and PCO-Y components exhibit a positive correlation with the β, increasing as the |β| rises. For the epochs with the local maxima of |β|, the formal error reaches 7.6 cm and 4.3 cm for the PCO-X and PCO-Y directions, reflecting a relatively bad

observational geometry. This phenomenon, which reflects the strong dependency of PCO estimates on the $|\beta|$, was also highlighted in [2], where similar patterns were observed and analyzed. For the C29 satellite, this β-dependent pattern is significantly weakened. Notably, this pattern is not necessary to be related to manufacturers. The maxima of $|\beta|$ is 63° and 35° for the C19 and C29 satellites, respectively, over the selected period. It is suggested that the higher $|\beta|$ causes a worse observability of PCO-X and PCO-Y components. In this light, a lower $|\beta|$ is assumed to be favorable for PCO estimation.
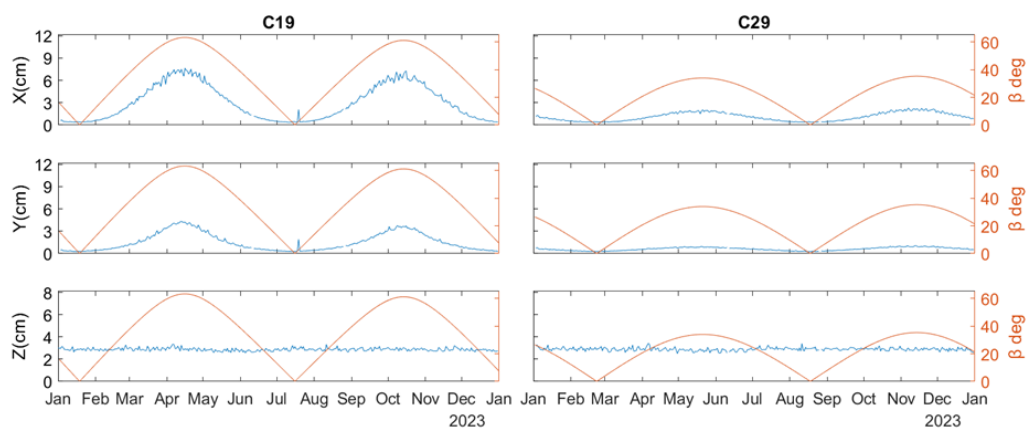
Figure 3. The formal errors of BDS-3 satellite PCO estimates as a function of the Sun elevation angles above orbital planes (β).

Figure 4 illustrates the daily BDS-3 satellite PCO estimates relative to the CSNO reference. Similar to the formal errors, the estimated PCO time series for the two selected satellites also show significant β-dependent variations for the PCO-X and PCO-Y components. For the C19 satellite, the absolute estimates for the PCO-X and PCO-Y components are generally less than 6 cm when $|\beta|$ is smaller than 25°, while are much more scattered when $|\beta|$ is larger than 32°. Though the C29 satellite shows a slightly smaller PCO-X and PCO-Y corrections, the β-dependent pattern still holds true. Together with Figure 4, it is concluded that bad observational geometry can significantly increase the uncertainty of PCO estimates for the PCO-X and PCO-Y components. Unlike the PCO-X and PCO-Y components, the PCO-Z component does not exhibit such a β-dependent pattern. These characteristics are consistent with the founding in [16].
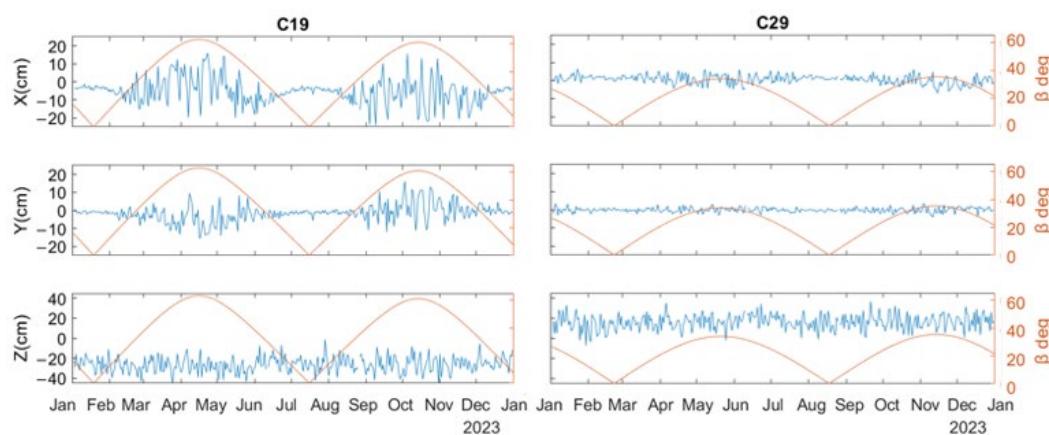
Figure 4. BDS-3 satellite PCO estimates relative to the CSNO reference as a function of the Sun elevation angles above orbital planes (β).

Figure 5 presents the PCO estimates in box–whisker plots, where the box indicates the interquartile range, the whiskers extend to 1.5 times the interquartile range, and outliers are shown as individual points. All satellites are grouped by manufacturers and orbit planes. The absolute values of PCO estimates for CAST satellites are roughly smaller than 10 cm and 5 cm for the PCO-X and PCO-Y directions, respectively. It is observed that the SECM satellites obtain more reliable PCO estimates within 10 cm for the two directions, which show minimal variation across different groups. However, the PCO-Z estimates exhibit large differences among satellites from different manufacturers and orbit planes. Most of the CAST satellites in the PL-B and PL-C planes display a negative bias of about −15~−20 cm, while the pair of C41/C42 satellites inversely have a position bias of about 20 cm. Concerning the SECM-A satellites, the PCO-Z estimates in the PL-A plane range from −25 cm to 25 cm, which is quite different from the negative values in the PL-C plane. These results underscore the necessity of considering satellite types and orbit planes when refining satellite antenna calibrations. In general, BDS-3 satellite PCO-Z estimates exhibits a systematic bias of −9.3 cm with respect to the CSNO reference, indicating a significant discrepancy between the estimated values in orbit and the ground calibrations before launch.
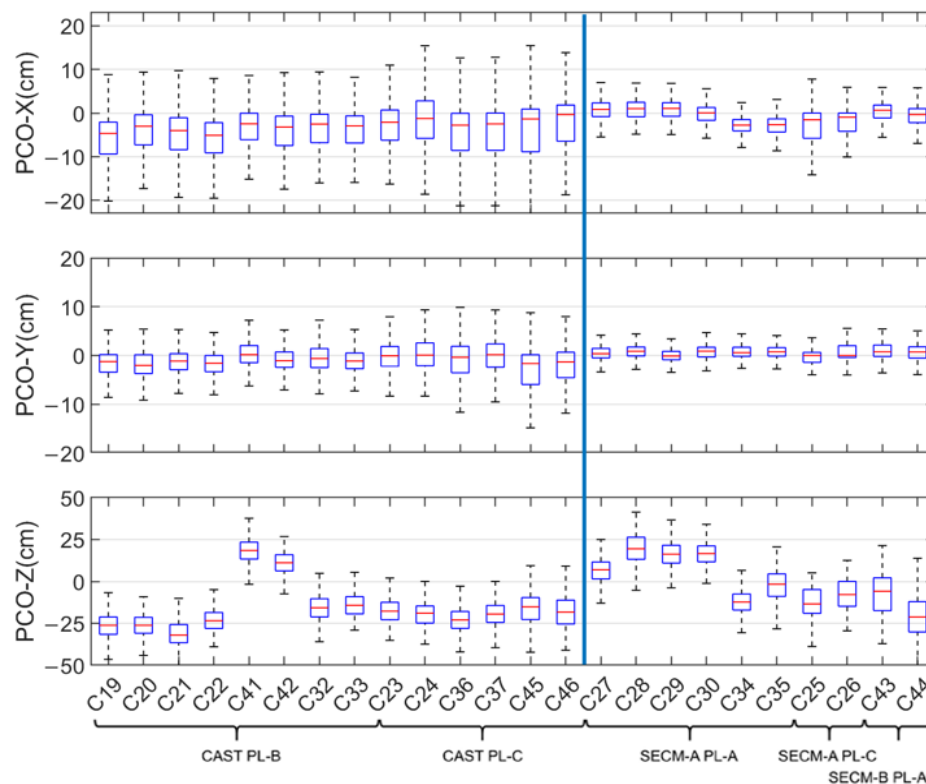
Figure 5. PCO corrections with respect to the CSNO values. CAST and SECM represent different satellite manufacturers, and PL-A, PL-B, and PL-C denote the orbital planes of the satellites. The blue lines distinguish satellites from the CAST and SECM manufacturers.

Table 3 provides the final PCO corrections for all BDS-3 MEO satellites. For the CAST satellites, the PCO-X values are mainly within −20~−26 cm, while two satellites C45 and C46 exhibit slightly larger values of −32.6 cm and −31.8 cm, respectively. With respect to the PCO-X component, the PCO-Y component presents much smaller offsets approximately ranging from −3.0 to −0.7 cm. The PCO-Z values range from approximately 165 cm to 190 cm. Compared to the CAST satellites, the SECM satellites present much smaller PCO corrections, whose PCO-X values are about 2.6~6.0 cm and PCO-Y values are only

−1.0~0.5 cm. Notably, the PCO-Z values show substantial variability between SECM-A and SECM-B groups, ranging from 89.8 cm to 130.9 cm. This result reflects potential design differences between SECM-A and SECM-B satellite structures.

Table 3. The estimated PCO values in cm for the linear combination of B1I/B3I signals.

Manu.	PRN	SVN	X	Y	Z
CAST	C19	C201	−25.7	−2.4	176.0
CAST	C20	C202	−25.6	−2.0	184.6
CAST	C21	C206	−24.1	−1.9	174.8
CAST	C22	C205	−24.9	−3.0	179.8
CAST	C23	C209	−22.2	−0.7	183.7
CAST	C24	C210	−20.9	0.1	185.8
CAST	C32	C213	−21.5	−1.5	189.7
CAST	C33	C214	−22.7	−1.9	189.7
CAST	C36	C218	−22.6	−2.0	165.5
CAST	C37	C219	−23.7	−1.9	167.2
CAST	C41	C227	−22.1	−1.3	176.9
CAST	C42	C228	−23.8	−2.1	170.3
CAST	C45	C223	−32.6	−2.8	179.4
CAST	C46	C222	−31.8	−2.4	178.8
SECM-A	C25	C212	4.1	−0.3	98.2
SECM-A	C26	C211	5.4	0.5	103.4
SECM-A	C27	C203	3.3	−0.1	118.4
SECM-A	C28	C204	3.3	0.4	130.9
SECM-A	C29	C207	3.5	−1.0	128.9
SECM-A	C30	C208	2.6	0.0	126.0
SECM-A	C34	C216	6.0	−0.2	99.3
SECM-A	C35	C215	5.9	−0.3	107.9
SECM-B	C43	C226	5.4	0.1	103.5
SECM-B	C44	C225	4.3	−0.2	89.8

Figure 6 compares the final PCO values in this study and the results from other studies, which are labeled as BUAA (this study), Yuan [17], Huang [16], and Zajdel [2]. All PCO results are computed using IF combination observations. One should keep in mind that [17] used the IGS20 frame, while Huang and Zajdel used the IGSR3 and IGS14 frames, respectively. Regarding the PCO-X component, the absolute values of BUAA PCO results are larger than those of other studies for the CAST satellites, while they are slightly smaller than those of other studies for the SECM satellites. The RMS of PCO-X differences stays at the level of 4.0 cm, 3.1 cm and 4.1 cm in terms of the RMS for Yuan, Huang, and Zajdel, respectively. The PCO-Y component presents a better consistency with the RMS of 0.7 cm, 0.6 cm, and 0.8 cm for Yuan, Huang, and Zajdel, respectively. Concerning the PCO-Z component, the results of this paper are generally smaller than the PCO values from the other studies. The RMS of PCO-Z differences is 10.9 cm, 21.3 cm, and 17.2 cm for Yuan, Huang, and Zajdel, respectively. It is obvious that our results are close to those of Yuan, while partial discrepancies exist with the results of Zajdel and Huang. This can be attributed to the fact that the PCOs from BUAA and Yuan were aligned with the same IGS20 frame, while Zajdel and Huang used the IGSR3 and IGS14 scale. Notably, certain satellites exhibit similar biases in their PCO-Z estimates like C27/C28 and C43/C44, which may be related to the extent of the uncertain quality of the SECM PCO calibrations [20].
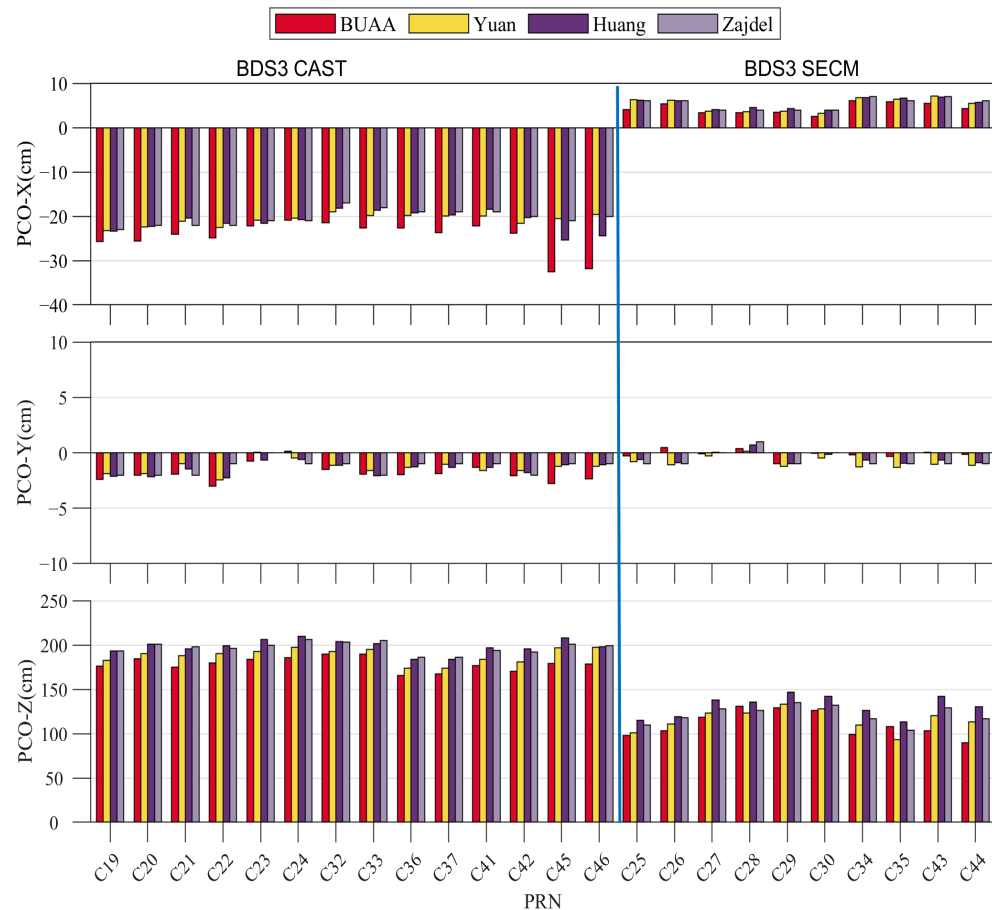
Figure 6. BDS-3 MEO satellite PCO estimates from different studies. BUAA is for this study. Yuan represents the value from [17]. Huang represents the value from [16]. Zajdel represents the value from [2]. The blue lines distinguish satellites from the CAST and SECM manufacturers.

3.2. Estimation of Station-Specific ISTPs

Figure 7 illustrates the station-specific ISTP estimates from GPS to BDS-3 systems in mean-error plots, where the "error" represents the STD of the ISTP time series. A total of 118 stations are categorized into 16 groups by the type of receiver antennas. Stations are sorted according to antenna types, with the variation in ISTP estimates serving as an indicator of the consistency within one antenna type. At first glance, most of the ISTP values approximately range from −5 to 5 mm for the North and East components and from −10 to 10 mm for the Up component. It is observed that the ISTP values depend on the different antenna types. Especially, the ISTP values derived from stations with the LEIAR25.R4 antenna show the best stability with the STD of 1.2, 1.5, and 2.9 mm for the North, East, and Up components, respectively. However, some distinct jumps are observed for individual stations among the stations using the same antenna type. This result suggests that the ISTP values are influenced by station-specific environmental factors, which may greatly relate to the GNSS-specific Troposphere Bias Parameter [18].
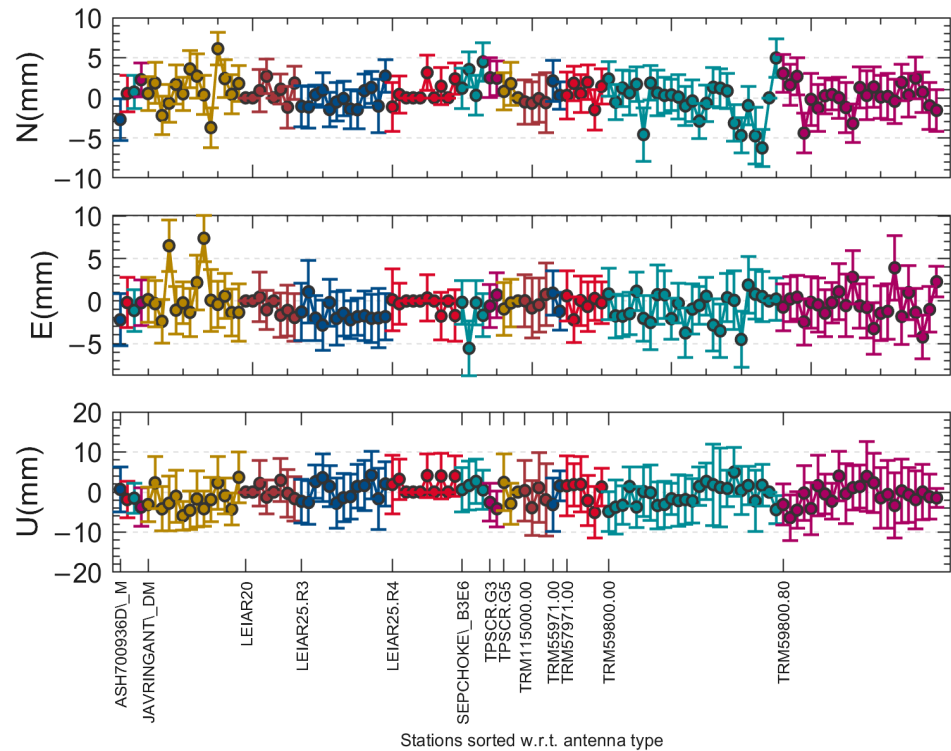
Figure 7. The station-specific ISTP estimates. Stations are categorized into 16 groups by the type of receiver antenna. Due to space constraints in the figure, certain antenna types between ASH700936D_M and JAVRINGANT_DM, including ASH701945B_M, ASH701945C_M, and ASH701945E_M, are not individually labeled.

Table 4 provides the mean and the STD of the ISTP estimates per antenna type in the North, East, and Up components. Though station-specific ISTP estimates vary among stations and antennas, the maximum of average ISTP values per antenna type is less than 3 mm for the horizontal component and less than 4 mm for the Up component. Considering all antenna types, the mean ISTP values are merely 0.6 mm, −0.6 mm, and −0.7 mm for the North, East, and Up components, respectively. This near-zero average indicates that, though individual antenna models may introduce distinct biases, the overall system remains relatively balanced when all antennas are considered collectively. Considering the visible variability of ISTP estimates among the stations with the same antenna type, a station-specific strategy for determining ISTP values is necessary to enhance the overall positioning accuracy.

Table 4. Average and STD of ISTP estimates for each antenna type (unit: mm).

Antenna Type	Station Number	N	E	U
ASH700936D_M	1	−2.7 ± 2.6	−2.2 ± 3.0	0.7 ± 5.6
ASH701945B_M	1	0.5 ± 2.3	−0.2 ± 3.0	−1.9 ± 4.5
ASH701945C_M	1	0.7 ± 2.1	−1.1 ± 2.5	−1.5 ± 3.8
ASH701945E_M	1	2.3 ± 2.1	−0.2 ± 2.7	−3.7 ± 4.8
JAVRINGANT_DM	1	1.1 ± 2.4	0.6 ± 2.9	−1.9 ± 5.5
LEIAR20	14	0.7 ± 1.4	−0.7 ± 1.7	0.2 ± 3.3
LEIAR25.R3	8	−0.2 ± 2.3	−1.6 ± 2.9	0.4 ± 5.8
LEIAR25.R4	13	0.6 ± 1.2	−0.3 ± 1.5	1.7 ± 2.9
SEPCHOKE_B3E6	10	2.4 ± 2.4	−1.9 ± 2.7	1.4 ± 5.5
TPSCR.G3	4	2.5 ± 2.3	0.1 ± 2.6	−3.4 ± 4.6
TPSCR.G5	2	0.9 ± 1.7	−0.4 ± 2.0	−0.2 ± 4.1

TRM115000.00	3	−0.5 ± 3.0	−0.1 ± 3.4	−1.1 ± 8.0
TRM55971.00	4	1.2 ± 2.1	−0.1 ± 2.4	−0.8 ± 5.2
TRM57971.00	2	0.8 ± 2.4	−0.4 ± 2.7	−0.1 ± 6.2
TRM59800.00	6	−0.5 ± 2.3	−0.8 ± 2.7	−0.7 ± 5.6
TRM59800.80	25	0.1 ± 2.6	−0.4 ± 3.0	−0.8 ± 6.4
Mean	--	0.6 ± 2.2	−0.6 ± 2.6	−0.7 ± 5.1

The STD of the ISTP estimates per antenna type reveals the variability of ISTP within the stations of the same antenna type. As shown in Table 5, certain antenna types, such as LEIAR25.R3 and TRM115000.00, display higher STD results with the maximum reaching up to 8 mm in the Up direction. Other antenna types, like LEIAR20 and LEIAR25.R4, show more stable ISTP estimates with the STD of about 3 mm, suggesting these antennas might introduce fewer systematic biases or might be less affected by local conditions. As a whole, the average STD of all antenna types is 2.2 mm, 2.6 mm, and 5.1 mm for the North, East, and Up components, respectively. It is observed that the Up component shows much more variations, indicating that the Up component is more sensitive to antenna model differences and environmental influences.

Table 5. Strategies adopted in PPP solutions.

Solutions	Satellite Products	Satellite PCOs	Station ISTPs
CODE-IGS	Precise products from CODE	igs20.atx	-
WHU-IGS	Precise products from WHU	igs20.atx	-
BUAA-IGS	Reprocessed using igs20.atx	igs20.atx	-
BUAA-EST	Reprocessed using the estimated PCOs	Values of this study	-
BUAA-EST-ISTP	Reprocessed using the estimated PCOs	Values of this study	Values of this study
Solutions	Satellite products	Satellite PCOs	Station ISTPs
CODE-IGS	Precise products from CODE	igs20.atx	-

In summary, the above analysis demonstrates the noticeable magnitude of ISTPs and their variations among different antenna types. Considering the potential discrepancy within the same antenna type, a station-specific strategy is used for ISTP estimation and correction.

3.3. Evaluation

In this section, we evaluate the impact of the resulting BDS-3 satellite PCOs and station-specific ISTPs by comparing the estimated terrestrial scale and station positions to those from the IGS20/igs20.atx framework. PPP solutions for a total of 118 stations (shown in Figure 2) are generated from 1 January 2023 to 31 December 2023. For comparison purpose, different PPP solutions were prepared, differing in the strategies of satellite precise products, satellite PCOs, and station-specific ISTPs. Table 5 summarizes the characteristics of the involved PPP solutions. The first three solutions, employing satellite products produced by the Center for Orbit Determination in Europe (CODE) [41], Wuhan University (WHU) [42], and this study, are denoted as COD-IGS, WHU-IGS, and BUAA-IGS. These solutions are based on igs20.atx, using ground-calibrated BDS-3 PCOs released by CSNO. The next solution used the reprocessed satellite products with the estimated satellite PCOs from this study being labeled as BUAA-EST. Following the BUAA-EST solution, the final BUAA-EST-ISTP solution, by further considering the ISTP corrections, was calculated. The resulting PPP station coordinates are compared to the IGS20 daily coordinates directly and by the Helmert transformation estimating three translations, three rotations, and a scale.

3.3.1. Terrestrial Scale

Figure 8 displays the scale parameter time series with respect to the IGS20 frame derived using BDS-3 observations with five different processing strategies. Table 6 summarizes the average scale and STD for each solution. It is found that all the three solutions using the BDS-3 antenna calibrations from igs20.atx obtain a positive scale, regardless of the satellite products. The mean scales are 0.51 ± 0.18 ppb, 0.46 ± 0.18 ppb, and 0.38 ± 0.20 ppb for CODE-IGS, WHU-IGS, and BUAA-IGS solutions, respectively. This scale bias with respect to the IGS20 frame is slightly better than [2], which showed the scale bias of about 0.55 ppb with respect to the IGS14 based on the BDS-3 B1I/B3I observations. The BDS-3 satellite products from CODE and WHU are produced together with other navigation constellations within the IGS20/igs20.axt framework, which contributes to improve the consistency of BDS-3 scale factor relative to the IGS20 frame. Compared to these two solutions, a smaller scale bias is obtained in the BUAA-IGS solution. The possible reason is that the BUAA satellite products and PPP station coordinates, which are calculated with the same software and background models, can reduce some potential discrepancy.
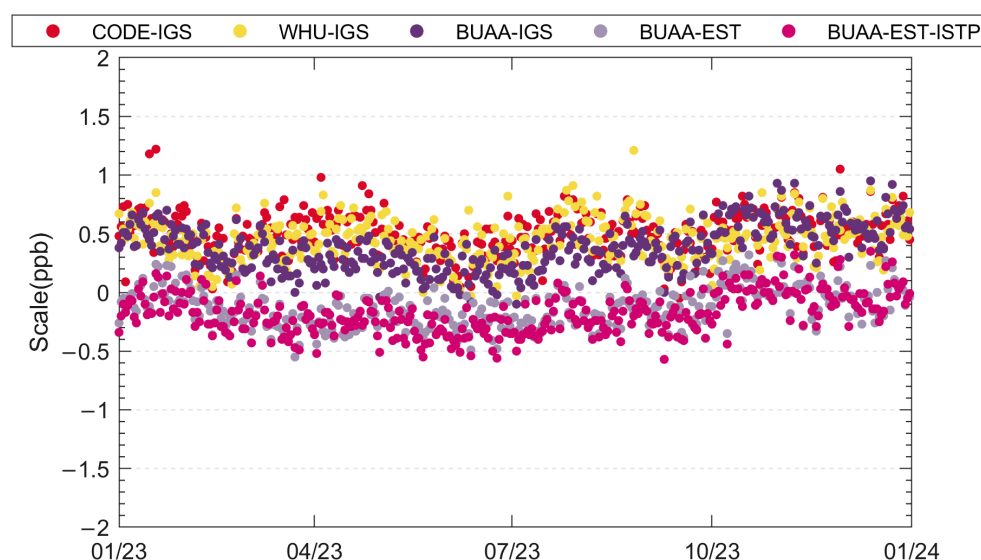
Figure 8. Time series of the scale bias between the CODE, WHU, and estimated PCO and ISTP solutions and the IGS20 reference frame scale. Table 5 shows the details on each solution. The format of time is month/year.

From Figure 8 and Table 6, an obvious offset is observed between the solutions using the IGS20 antenna calibrations and the estimated BDS-3 PCOs. The two solutions using the estimated BDS-3 PCOs have a negative scale with respect to the IGS20 frame, meaning that the estimated coordinates are below the IGS20 frame. The BUAA-EST and BUAA-EST-ISTP solutions presents a scale bias of −0.12 ± 0.17 and −0.18 ± 0.17 ppb, respectively. This bias delivers a decent agreement with [17], which reported the −0.15 ± 0.23 ppb bias with respect to the IGS20 frame based on BDS-3-only observations. This result indicates that the estimated BDS-3 satellite PCOs are well calibrated to the IGS20 frame. When using the estimated BDS-3 PCOs, the additional ISTP corrections for station coordinates induce a disagreement of 0.06 ppb in terrestrial scale. This imperceptible change is compatible with the mean ISTP value of −0.7 mm for the Up component.

Table 6. Terrestrial scale with respect to IGS20 frame.

Solution	Scale (ppb)
CODE-IGS	0.51 ± 0.18
WHU-IGS	0.46 ± 0.18
BUAA-IGS	0.38 ± 0.20
BUAA-EST	−0.12 ± 0.17
BUAA-EST-ISTP	−0.18 ± 0.17

3.3.2. Station Coordinates

The daily RMS of PPP station coordinates with respect to IGS20 daily solutions without and with the Helmert transformation are illustrated in Figure 9 and Figure 10, respectively. For a quantitative statistic, Table 7 summarizes the mean RMS for all schemes. It can be seen that the solutions using the BDS-3 satellite PCOs from igs20.atx show differences with respect to IGS20 daily solutions. Before the Helmert transformation, the RMS of CODE-IGS and WHU-IGS solutions is about 3.4~4.5 mm for the horizontal component and 8.5 mm for the Up component. These values are slightly larger than the result of the BUAA-IGS solution, which is 3.0~3.1 mm for the horizontal component and 7.0 mm for the Up component. The improved station coordinates from the BUAA-IGS solution can be attributed to the high consistency of background models used when determining satellite orbits and station coordinates. With the Helmert transformation, the above solutions achieve a better agreement with respect to IGS20 coordinates. For the most concerned Up component, the station differences are significantly reduced by about 14.1%, 18.8%, and 14.3% for the CODE-IGS, WHU-IGS, and BUAA-IGS solutions with the RMS of 7.3 mm, 6.9 mm, and 6.0 mm, respectively.

Table 7. RMS of PPP station coordinates with respect to IGS20 daily solutions.

Solution	Without Helmert Transformation (mm)			With Helmert Transformation (mm)		
	N	E	U	N	E	U
CODE-IGS	3.4	3.9	8.5	3.1	3.4	7.3
WHU-IGS	4.5	3.6	8.5	3.3	3.1	6.9
BUAA-IGS	3.0	3.1	7.0	2.8	2.9	6.0
BUAA-EST	3.2	3.1	6.2	2.8	2.8	5.7
BUAA-EST-ISTP	2.3	2.7	5.2	2.3	2.4	5.0

Comparing the BUAA-IGS and BUAA-EST solution before the Helmert transformation, it is observed that the estimated BDS-3 satellite PCOs mainly contribute to the Up component with the RMS reduced to 6.2 mm, obtaining an improvement of 11.4%. For the BUAA-EST solution, the impact of the Helmert transformation is merely 0.5 mm for the Up component. This result indicates that the station coordinates based on the estimated BDS-3 satellite PCOs are compatible with the IGS20 coordinates. In addition, the scale bias of BUAA-EST solution with respect to the IGS20 frame stays at the level of −0.12 ppb, proving that our estimated BDS-3 satellite PCOs are in a good agreement with the IGS20 scale.

Among the analyzed solutions, the BUAA-EST-ISTP solution with station-specific ISTPs achieves the smallest RMS of station coordinates, which is 2.3, 2.7, and 5.2 mm without the Helmert transformation for the North, East, and Up components, respectively. The additional correction of station-specific ISTPs reduced the RMS by 28.1%, 12.9%, and 16.1% for the North, East, and Up components, respectively. Since the estimated BDS-3

satellite PCOs and station-specific ISTPs corrections already improved the consistency between BDS-3-derived station coordinates and IGS20 frame, only a slight decrease in RMS is observed after the Helmert transformation. Finally, given the obvious impact of station-specific ISTPs on station coordinates, it is suggested that the operational multi-GNSS products should take this offset into consideration.
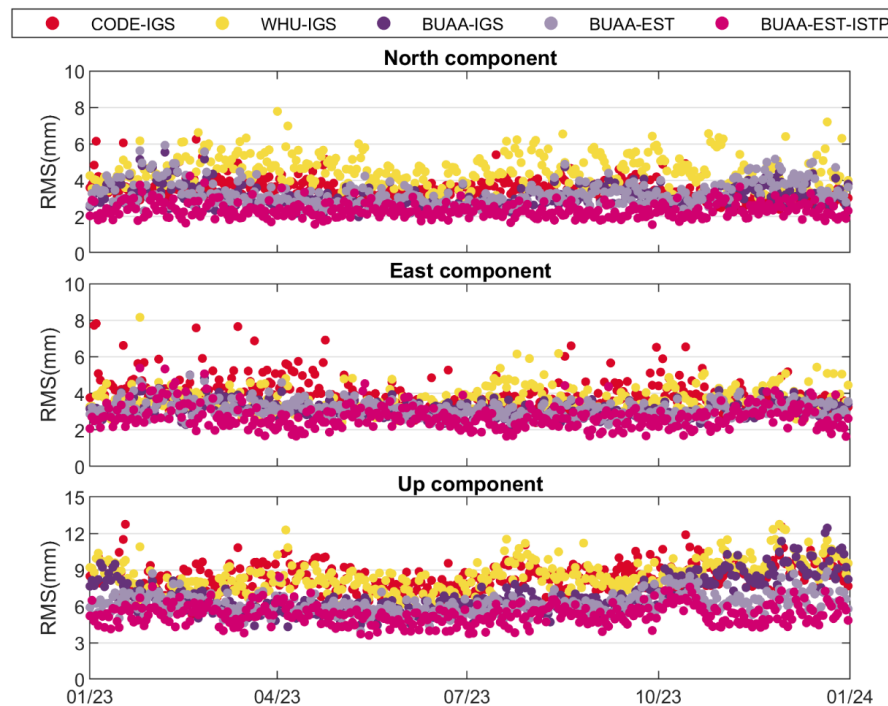
Figure 9. RMS statistics of daily positioning results relative to IGS daily solutions without Helmert transformation.
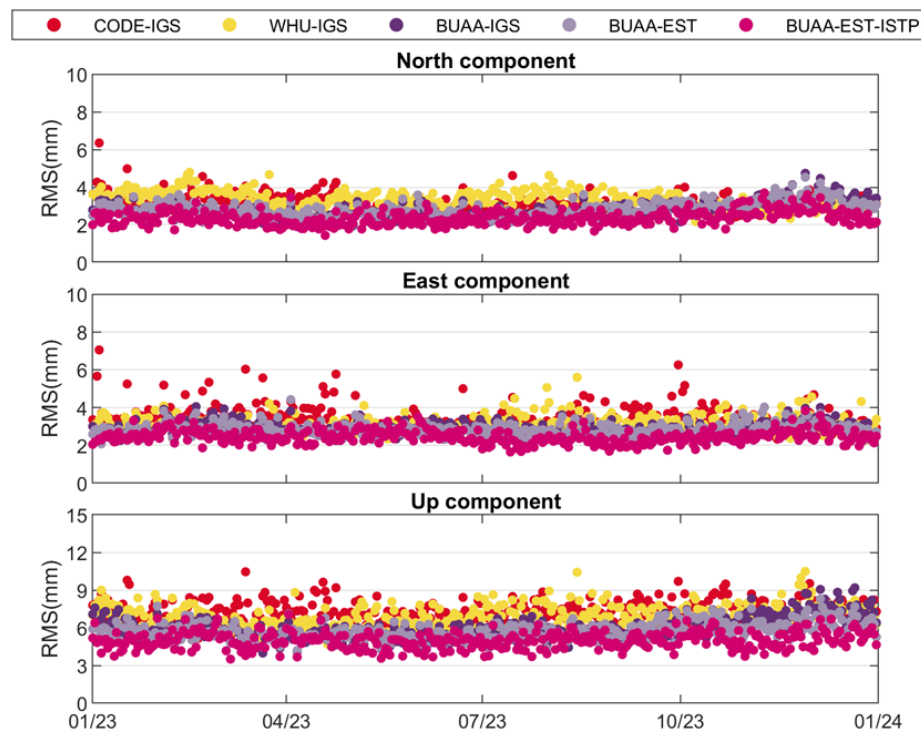
Figure 10. RMS statistics of daily positioning results relative to IGS daily solutions with Helmert transformation.

The improvement in positioning precision observed in this study is primarily attributed to the refined estimation of BDS satellite PCOs. By calibrating the PCOs to align with the IGS20 reference frame, the systematic geometric errors between the satellite antenna phase center and the receiver are reduced. This correction enhances the accuracy of satellite-receiver distance calculations and the solution consistent with the IGS20 framework. The alignment of BDS PCOs with IGS20 provides a stable foundation for multi-GNSS integration, ultimately improving the precision and reliability of station coordinate estimates.

Similarly, the incorporation of ISTP estimation is effective in mitigating unmodeled station biases. These biases propagate through multi-GNSS solutions, influencing the accuracy of BDS-derived coordinates. By modeling and estimating ISTPs, this study effectively compensates for these discrepancies, ensuring BDS and other constellations are compatible. This approach improves the precision of the positioning results, as evidenced by enhanced positioning performance with the IGS20 reference frame. Together, these refinements indicate the importance of addressing both satellite- and receiver-related factors to achieve the high-precision positioning performance of BDS.

4. Conclusions

Precise station coordinates are essential for using GNSS to study subtle geophysical signals and processes. However, the positioning accuracy of BDS-3 is still inferior to that of other GNSS constellations. On the one hand, the BDS-3 satellite antenna PCOs released by the CSNO are not fully compatible with the IGS20/igs20.atx framework, resulting in the discrepancy of terrestrial scale between the BDS-3-derived station coordinates and IGS20 products. On the other hand, the so-called ISTPs increase the inconsistency of station coordinates derived from BDS-3 and GPS observations. This study aims to enhance BDS-3-derived station coordinates by utilizing calibrated satellite antenna PCOs and station-specific ISTPs.

The BDS-3 satellite PCOs were estimated using the NNS constraint to IGS20 daily solutions. Analysis reveals a clear dependence of the PCO-X and PCO-Y components on the Sun elevation angle (β), with higher $|\beta|$ values leading to increased formal errors and worse observability. In contrast, the PCO-Z component shows no β-dependence but exhibits variations among satellites from different manufacturers and orbit planes. Overall, the PCO estimates are consistent with Yuan et al. (2024) under the IGS20/igs20.atx framework. The application of these antenna models reduced the scale difference in BDS-3 station coordinates with respect to IGS20 from 0.38 ppb to −0.12 ppb, improving consistency by 68.4%. Similarly, the RMS of station coordinate differences in the Up component decreased from 7.0 mm to 6.2 mm, obtaining an improvement of 11.4%. These results demonstrate that the estimated BDS-3 PCOs are compatible with the IGS20 frame and contribute to improved station coordinate accuracy.

The station-specific ISTP estimates exhibit significant variability across receiver antenna types, with most values ranging from −5 to 5 mm for horizontal components and −10 to 10 mm for the Up component, suggesting that antenna types notably influence the stability of ISTP estimates. Station-specific environmental factors can cause inconsistencies among stations using the same antenna and occasionally cause abrupt jumps in the ISTP values of certain individual stations. Based on the estimated BDS-3 satellite PCOs, the inclusion of ISTP corrections in the solution improves positioning accuracy. Finally, the RMS of station coordinate differences with respect to IGS20 products is 2.3 mm, 2.7 mm, and 5.2 mm for the North, East, and Up components, respectively. Compared to the solution using only the estimated BDS-3 satellite PCOs, the consistency is improved by 0.9 mm, 0.4 mm, and 1.0 mm for the respective components.

References

1. Yang, Y.; Tang, J.; Montenbruck, O. Chinese Navigation Satellite Systems. In *Springer Handbook of Global Navigation Satellite Systems*; Teunissen, P.J.G., Montenbruck, O., Eds.; Springer International Publishing: Cham, Switzerland, 2017; pp. 273–304, ISBN 978-3-319-42928-1.

2. Zajdel, R. On the Potential Contribution of BeiDou-3 to the Realization of the Terrestrial Reference Frame Scale. *GPS Solut.* **2022**, *26*, 109.

3. Peng, Y.; Lou, Y.; Dai, X.; Guo, J.; Shi, C. Impact of Solar Radiation Pressure Models on Earth Rotation Parameters Derived from BDS. *GPS Solut.* **2022**, *26*, 126. https://doi.org/10.1007/s10291-022-01316-1.

4. Guo, S.; Fan, L.; Wei, N.; Gu, S.; Fang, X.; Jing, G.; Shi, C. Impact of Satellite Clock Modeling on the GNSS-Based Geocenter Motion Determination. *J. Geod.* **2024**, *98*, 70. https://doi.org/10.1007/s00190-024-01879-6.

5. Riguzzi, F.; Devoti, R.; Pietrantonio, G. GNSS Data Provide Unexpected Insights in Hydrogeologic Processes. *Bull. Geophys. Oceanogr.* **2021**, *62*, 637–646.

6. Bock, Y.; Melgar, D. Physical Applications of GPS Geodesy: A Review. *Rep. Prog. Phys.* **2016**, *79*, 106801.

7. Kouba, J.; Lahaye, F.; Tétreault, P. Precise Point Positioning. In *Springer Handbook of Global Navigation Satellite Systems*; Teunissen, P.J.G., Montenbruck, O., Eds.; Springer International Publishing: Cham, Switzerland, 2017; pp. 723–751, ISBN 978-3-319-42928-1.

8. Shi, J.; Ouyang, C.; Huang, Y.; Peng, W. Assessment of BDS-3 Global Positioning Service: Ephemeris, SPP, PPP, RTK, and New Signal. *GPS Solut.* **2020**, *24*, 81. https://doi.org/10.1007/s10291-020-00995-y.

9. Johnston, G.; Riddell, A.; Hausler, G. The International GNSS Service. In *Springer Handbook of Global Navigation Satellite Systems*; Teunissen, P.J.G., Montenbruck, O., Eds.; Springer International Publishing: Cham, Switzerland, 2017; pp. 967–982.

10. Rebischung, P.; Altamimi, Z.; Métivier, L.; Collilieux, X.; Gobron, K.; Chanard, K. Analysis of the IGS Contribution to ITRF2020. *J. Geod.* **2024**, *98*, 49.

11. CSNO Satellite Antenna Phase Center of BDS. Available online: http://www.beidou.gov.cn/yw/gfgg/201912/t20191209_19613.html (accessed on 26 November 2024).

12. Xia, F.; Ye, S.; Chen, D.; Wu, J.; Wang, C.; Sun, W. Estimation of Antenna Phase Center Offsets for BeiDou IGSO and MEO Satellites. *GPS Solut.* **2020**, *24*, 90. https://doi.org/10.1007/s10291-020-01002-0.

13. Qu, Z.; Guo, J.; Zhao, Q. Phase Center Corrections for BDS IGSO and MEO Satellites in IGb14 and IGSR3 Frame. *Remote Sens.* **2021**, *13*, 745. https://doi.org/10.3390/rs13040745.

14. Zhu, S.Y.; Massmann, F.-H.; Yu, Y.; Reigber, C. Satellite Antenna Phase Center Offsets and Scale Errors in GPS Solutions. *J. Geod.* **2003**, *76*, 668–672. https://doi.org/10.1007/s00190-002-0294-1.

15. Huang, G. Estimation of Antenna Phase Center Offset for BDS IGSO and MEO Satellites. *GPS Solut.* **2018**, *22*, 49.

16. Huang, C.; Song, S.; He, L.; Chen, Q.; Jiao, W.; Zhou, W.; Jiao, G.; Zhao, H.; Yang, Y. Estimation of Antenna Phase Center Offsets for BDS-3 Satellites with the Metadata and Receiver Antenna Calibrations. *J. Geod.* **2023**, *97*, 57. https://doi.org/10.1007/s00190-023-01757-7.

17. Yuan, Y.; Li, X.; Yao, Y.; Huang, S.; Wang, Q.; Zhang, K. Estimation of Phase Center Corrections for BDS Satellites Aligned to the IGS20 Frame. *GPS Solut.* **2024**, *28*, 63. https://doi.org/10.1007/s10291-023-01603-5.

18. Villiger, A.; Dach, R.; Schaer, S.; Prange, L.; Zimmermann, F.; Kuhlmann, H.; Wuebbena, G.; Schmitz, M.; Beutler, G.; Jaggi, A. GNSS Scale Determination Using Calibrated Receiver and Galileo Satellite Antenna Patterns. *J. Geod.* **2020**, *94*, 93. https://doi.org/10.1007/s00190-020-01417-0.

19. Schaer, S.; Meindl, M. Consideration of Station-Specific Intersystem Translation Parameters at CODE. In Proceedings of the EUREF 2011 Symposium, Chisinau, Moldova, 25–28 May 2011.

20. Zajdel, R.; Sośnica, K.; Dach, R.; Bury, G.; Prange, L.; Jäggi, A. Network Effects and Handling of the Geocenter Motion in Multi-GNSS Processing. *JGR Solid Earth* **2019**, *124*, 5970–5989. https://doi.org/10.1029/2019JB017443.

21. Rebischung, P.; Schmid, R. IGS14/Igs14.Atx: A New Framework for the IGS Products. In Proceedings of the American Geophysical Union, Fall Meeting 2016, San Francisco, CA, USA, 12–16 December 2016.

22. Dach, R.; Selmke, I.; Villiger, A.; Arnold, D.; Prange, L.; Schaer, S.; Sidorov, D.; Stebler, P.; Jäggi, A.; Hugentobler, U. Review of Recent GNSS Modelling Improvements Based on CODEs Repro3 Contribution. *Adv. Space Res.* **2021**, *68*, 1263–1280. https://doi.org/10.1016/j.asr.2021.04.046.

23. Villiger, A.; Dach, R. International GNSS Service: Technical Report 2019. 2020. Available online: https://igs.org/igs-2019-technical-report-is-now-available/ (accessed on 1 October 2024).

24. Schmid, R.; Steigenberger, P.; Gendt, G.; Ge, M.; Rothacher, M. Generation of a Consistent Absolute Phase-Center Correction Model for GPS Receiver and Satellite Antennas. *J. Geod.* **2007**, *81*, 781–798. https://doi.org/10.1007/s00190-007-0148-y.

25. Rothacher, M.; Schmid, R. ANTEX: The Antenna Exchange Format, Version 1.4. Available online: https://files.igs.org/pub/data/format/antex14.txt (accessed on 1 October 2024).

26. Shi, C.; Guo, S.; Fan, L.; Gu, S.; Fang, X.; Zhou, L.; Zhang, T.; Li, Z.; Li, M.; Li, W.; et al. GSTAR: An Innovative Software Platform for Processing Space Geodetic Data at the Observation Level. *Satell. Navig.* **2023**, *4*, 18. https://doi.org/10.1186/s43020-023-00109-2.

27. Zhao, Q.; Guo, J.; Wang, C.; Lyu, Y.; Xu, X.; Yang, C.; Li, J. Precise Orbit Determination for BDS Satellites. *Satell Navig.* **2022**, *3*, 2. https://doi.org/10.1186/s43020-021-00062-y.

28. Montenbruck, O.; Steigenberger, P.; Prange, L.; Deng, Z.; Zhao, Q.; Perosanz, F.; Romero, I.; Noll, C.; Stürze, A.; Weber, G.; et al. The Multi-GNSS Experiment (MGEX) of the International GNSS Service (IGS)–Achievements, Prospects and Challenges. *Adv. Space Res.* **2017**, *59*, 1671–1697. https://doi.org/10.1016/j.asr.2017.01.011.

29. Steigenberger, P.; Fritsche, M.; Dach, R.; Schmid, R.; Montenbruck, O.; Uhlemann, M.; Prange, L. Estimation of Satellite Antenna Phase Center Offsets for Galileo. *J. Geod.* **2016**, *90*, 773–785. https://doi.org/10.1007/s00190-016-0909-6.

30. Arnold, D.; Meindl, M.; Beutler, G.; Dach, R.; Schaer, S.; Lutz, S.; Prange, L.; Sośnica, K.; Mervart, L.; Jäggi, A. CODE's New Solar Radiation Pressure Model for GNSS Orbit Determination. *J. Geod.* **2015**, *89*, 775–791. https://doi.org/10.1007/s00190-015-0814-4.

31. Pavlis, N.; Kenyon, S.; Factor, J.; Holmes, S. Earth gravitational model 2008. In *SEG Technical Program Expanded Abstracts 2008*; Society of Exploration Geophysicists: Houston, TX, USA, 2008; pp. 761–763.

32. Standish, E.M. JPL planetary and lunar ephemerides. *IOM* **1998**, *312*, F-98-048.

33. Lyard, F.; Lefevre, F.; Letellier, T.; Francis, O. Modelling the global ocean tides: modern insights from FES2004. *Ocean. Dyn.* **2006**, *56*, 394–415.

34. Petit, G. IERS Conventions (2010). 2010. Available online: https://www.researchgate.net/profile/Gerard-Petit/publication/235112142_IERS_conventions_2010/links/09e41510fd516c4924000000/IERS-conventions-2010.pdf (accessed on 1 October 2024).

35. Rodriguez-Solano, C.J.; Hugentobler, U.; Steigenberger, P.; Lutz, S. Impact of Earth radiation pressure on GPS position estimates. *J. Geod.* **2012**, *86*, 309–317.

36. Steigenberger, P.; Thoelert, S.; Montenbruck, O. GNSS Satellite Transmit Power and Its Impact on Orbit Determination. *J. Geod.* **2018**, *92*, 609–624. https://doi.org/10.1007/s00190-017-1082-2.

37. Saastamoinen, J. Atmospheric correction for the troposphere and stratosphere in radio ranging satellites. *Use Artif. Satell. Geod.* **1972**, *15*, 247–251.

38. Boehm, J.; Werl, B.; Schuh, H. Troposphere mapping functions for GPS and very long baseline interferometry from European Centre for Medium-Range Weather Forecasts operational analysis data. *J. Geophys. Res. Solid Earth* **2006**, *111*, B02406.

39. Lagler, K.; Schindelegger, M.; Böhm, J.; Krásná; H; Nilsson, T. GPT2: Empirical slant delay model for radio space geodetic techniques. *Geophys. Res. Lett.* **2013**, *40*, 1069–1073.

40. Ge, M.; Gendt, G.; Dick, G.; Zhang, F.P. Improving Carrier-Phase Ambiguity Resolution in Global GPS Network Solutions. *J. Geod.* **2005**, *79*, 103–110. https://doi.org/10.1007/s00190-005-0447-0.

41. Prange, L.; Orliac, E.; Dach, R. Others CODE's Five-System Orbit and Clock Solution—The Challenges of Multi-GNSS Data Analysis. *J. Geod.* **2016**, *91*, 345–360.

42. Guo, J.; Xu, X.; Zhao, Q.; Liu, J. Precise Orbit Determination for Quad-Constellation Satellites at Wuhan University: Strategy, Result Validation, and Comparison. *J. Geod.* **2016**, *90*, 143–159. https://doi.org/10.1007/s00190-015-0862-9.